Structure of the Cs-induced (1×3) reconstruction of Au(110)

Patricio Häberle and Paul Fenter
Department of Physics and Laboratory for Research on the Structure of Matter, University of Pennsylvania, Philadelphia, Pennsylvania 19104
and Department of Physics and Astronomy, P.O. Box 849, Rutgers–The State University of New Jersey, Piscataway, New Jersey 08854

Torgny Gustafsson
Department of Physics and Astronomy, P.O. Box 849, Rutgers–The State University of New Jersey, Piscataway, New Jersey 08854
(Received 31 May 1988)

The clean Au(110) surface exhibits a (1×2) reconstruction with an atomic arrangement corresponding to a missing-row (MR) structure. By depositing Cs on this surface, we have formed two new structures with (1×5) and (1×3) low-energy electron diffraction (LEED) patterns, corresponding to Cs coverages of (3±2)% and (5^{+6}_{-2})% of a monolayer, respectively. The superstructures therefore correspond to further substrate reconstructions. We have used medium-energy ion scattering (MEIS) with channeling and blocking to study the structure of the (1×3) reconstruction. Our results show a clear indication of a missing-row-type structure which displays long and narrow (111) microfacets that go deep into the crystal. The most important surface distortions are an inwards relaxation of the first layer by 22%, and a large buckling in the third layer. Other subsurface rearrangements are such that they produce a slight smoothing of this highly corrugated structure. These results are discussed in the light of recent theoretical calculations of the total energy of the fcc (110) surfaces. In these calculations the relative stability of the different surface geometries is dominated by the *s-p* electrons at the surface. For the Cs/Au system, a charge transfer from the alkali to the Au substrate alters the energy distribution of these electrons and shifts the equilibrium geometry from the (1×2) MR to the observed (1×3) structure.

I. INTRODUCTION

The best known reconstructions on clean metal surfaces occur in two regions of the Periodic Table. The (100) surfaces of the isoelectronic bcc metals Mo and W show a well-known reversible (2×2) low-temperature reconstruction, while the (110) surfaces of the 5*d* fcc metals Ir, Pt and Au are reconstructed at room temperature. This reconstruction doubles the periodicity of the surface along the [001] direction, which results in a (1×2) low-energy electron diffraction (LEED) pattern. The fact that Mo and W belong to the same column in the Periodic Table and therefore are isoelectronic is frequently taken as an indication that the reconstruction has a common origin for both metals. Corresponding evidence is not as clear in the case of the Ir, Pt, and Au reconstructions as they instead belong to the same row in the Periodic Table and the electronic structure around the Fermi level is therefore different for the three metals.

The (1×2) reconstructions of Ir(110), Pt(110), and Au(110) are known to be of the missing-row (MR) type, i.e., every other closed-packed row of atoms along the [$\bar{1}$10] direction in the surface layer has been removed.[1] The experimental evidence is particularly clear for the Au(110) surface. Here, LEED (Ref. 2) and medium-energy ion scattering (MEIS) (Ref. 3) have shown that the MR reconstruction is accompanied by a large inwards movement of the first layer of atoms and a buckling of the third layer, resulting in an overall smoothing of the surface. Recent LEED work on Ir(110),[4] as well as MEIS data on Ir(110),[5] and Pt(110),[6] show very similar results.

The clean (110) surfaces of Cu, Ag, and Pd show (1×1) LEED patterns, but can be made to reconstruct to a (1×2) unit cell with the adsorption of submonolayer amounts of alkali metals.[7–10] These new structures have also been shown to correspond to missing-row reconstructions. It is an intuitively appealing idea that both the clean 5*d* reconstructions and the alkali-metal-induced ones are caused by the same mechanism. A recent total-energy calculation by Ho and Bohnen using a pseudopotential density functional formalism suggests that the stabilization of the MR reconstruction on Au(110) comes about mainly due to the need to lower the kinetic energy of the *s-p* electrons at the surface.[11] Any constraint in the available volume of an electron tends to increase its kinetic energy. The effective volume available for the *s-p* electrons is limited by the size of the lattice and the room left over by the *d* orbitals. Since the 5*d* orbitals are larger than the 3*d* and in particular the 4*d*, this leaves less room for the *s-p* electrons in the 5*d* metals, requiring a major surface rearrangement to reduce the confinement and kinetic energy of these electrons. This picture is consistent with results from theoretical calculations, which show that the (1×1) (110) surfaces of the 3*d* and, in particular, the 4*d* fcc metals are only marginally stable.[12] Within this framework we can explain the alkali-metal-induced reconstructions in terms of a charge transfer from the adsorbed alkali metal to the substrate. This additional charge will increase the density and pressure of the *s-p* electrons at the surface. This increase in the pressure,

which in the case of the 5*d* metals is a manifestation of the larger size of the 5*d* orbitals, induces the same type of reconstruction on the 3*d* and 4*d* metals. The calculation by Ho and Bohnen[11] is but one of several recent total-energy calculations for the fcc (110) surfaces.[12–15] All these calculations show a substantially lower energy for the MR (1×2) Au(110) structure than for the (1×1) surface, but the energies of higher-order reconstructions [(1×3), (1×4), etc.] are calculated to be very close to, and in some cases actually lower than, the (1×2) surface.[12] In these reconstructions, additional rows of atoms are missing from the surface and also from subsurface layers, resulting in long microfacets normal to the [111] direction. Based on the discussion above, it would appear very plausible that additional *s* charge could change the balance in the delicate equilibrium between the (1×2) reconstruction and the higher-order reconstructions. It is therefore interesting to study the influence of alkali-metal deposition on the (1×2) surface reconstruction of Au(110).

Below, we present the first experimental structural study of one of these higher-order superstructures, the Cs-induced (1×3) reconstruction of Au(110). We propose a detailed model for the surface structure based on data from medium-energy ion scattering. Moritz and Wolf have briefly reported the observation of a (1×3) structure on a partially annealed Au(110) surface.[16] Also, Held *et al.* have observed a (1×3) LEED pattern on Au(110).[17] Finally, Morgante *et al.* have observed a (1×3) pattern caused by alloying approximately half a monolayer of Ag with a Au(110) substrate.[18] The present investigation appears to be the first one in which a well-characterized (1×3) reconstruction of Au(110) has been observed.

In Sec. II, we describe briefly our experimental setup and procedures. The results are reported in Sec. III, and in Sec. IV we give some concluding remarks.

II. EXPERIMENT

The strength of ion scattering as a tool for surface structural studies lies in the fact that the ion-surface interaction law is well known in the energy range we use—essentially only elementary Rutherford scattering is involved—so that the outcome of an experiment on a hypothetical arrangement of surface atoms can be modeled accurately. As the experimental scattering yield can be measured in absolute units, calculation and experiment can be compared without scaling factors, and any remaining discrepancies between the two can therefore be attributed to inaccuracies in the structural model. Another useful advantage of MEIS is that by merely inspecting the data, it is in simple cases possible to obtain evidence for, say, the sign of the change in some important structural parameter.[1]

Energetic ions incident on a crystal along a low index crystallographic direction are predominantly channeled. The Coulombic interaction between ions and atoms in the crystal will deflect the incident ions. This will create regions, known as shadow cones, inside the crystal which are free from traveling ions. Consequently, the vast majority of ions are forced into channels that can go deep into the crystal.

A small fraction of the incident ions will undergo large angle scattering, not only from atoms in the top layer but also from the next few layers of the crystal. The main dechanneling mechanisms are structural distortions and thermal vibrations at the surface, which allow atoms in deeper layers to become visible to the incident ion beam. These deeper layer atoms can vibrate out of the shadow cones into the ion channels, resulting in large-angle-scattering events. The yield of backscattered ions will therefore contain information about distortions in the surface as well as the surface vibrational properties. This forms the basis of the channeling technique for surface structural studies.

One can often obtain even more detailed information by measuring the angular distribution of the backscattered ion yield. An ion scattered from an atom in a subsurface layer can be blocked on its way out by an atom closer to the surface. This will lower the yield along the direction joining the two atoms and produce a *blocking dip* in the scattered yield. This particular scattering geometry is referred to as "double alignment" because the ion beam is aligned with a channeling direction and the detector with a blocking direction. The technique is commonly known as *channeling and blocking.*[1]

The data presented below are in the form of a normalized yield of backscattered ions as a function of scattering angle. We normalize the raw data by dividing by a screened Rutherford-scattering cross section. The yield is then placed on an absolute scale by comparing to backscattering data from a standard, a Si wafer with an implanted Sb density of 0.49 atoms/Å^2. The yield is expressed as the number of atoms per Au(110)-(1×1) unit-cell (1 monolayer = 8.5×10^{14} atoms/cm^2) visible to the detector at a particular scattering angle.

To get quantitative structural information from MEIS it is necessary to perform Monte Carlo simulations. Using the known cross section we can predict the absolute yield in any scattering geometry for a particular surface structure. The structural parameters are varied, and the calculation repeated. The search for the optimum set of structural parameters is done using an *R*-factor analysis as described previously.[3,6]

The Au(110) sample was electropolished in a cyanide solution and then mounted on a high-precision manipulator in an ultrahigh-vacuum (UHV) system with a base pressure less than 10^{-10} Torr. This chamber, which contained facilities for LEED and Auger spectroscopy with a cylindrical mirror analyzer, was connected through a differentially pumped beam line to a 180-keV ion accelerator.[19] The scattered ions were detected using an electrostatic toroidal analyzer with a position-sensitive detector. The energy resolution was 0.65 keV at 100 keV and the total angular resolution $\approx0.2°$. The sample was cleaned by successive cycles of Ne^+ sputtering and annealing to ≈800 K. It showed a clear and distinct (1×2) LEED pattern.

The Cs source (SAES Getters USA) was carefully degassed in a separate vacuum chamber and then moved into the main chamber without breaking vacuum. The

pressure stayed below 4×10^{-10} Torr during Cs deposition. After deposition at room temperature the LEED pattern showed streaks in a direction consistent with surface disorder perpendicular to the closed-packed rows and also an increase in the background intensity. A subsequent anneal to ≈500 K reduced the background and produced a clear (1×3) LEED pattern. By depositing a larger amount of Cs it was also possible to form a lower quality (1×3) pattern without annealing. The cleanliness of the deposited layer was verified with Auger spectroscopy. The Cs signal in the backscattering spectra was used to determine an absolute scale for the coverages, against which the Cs Auger intensities were calibrated. Using the procedure of deposition followed by annealing we were also able to obtain a (1×5) LEED pattern at a coverage of $\approx(3\pm2)\%$ of a monolayer and the (1×3) LEED pattern mentioned above at $(5^{+6}_{-2})\%$ of a monolayer. The large error bars on the absolute converges reflect the fact that the weak Cs signal in the ion scattering spectrum lies on top of a strong Au signal. The relative coverages of the two structures are known with a much greater accuracy.

The (1×5) LEED pattern exhibited a very high background intensity, which suggests significant disorder. Total-energy calculations on Au(110) have given the result that the only structure more stable than a (1×5) MR is the (1×2) MR.[15] Because of the disorder, we performed no structural analysis on this phase.

III. RESULTS

A top view of the (1×2) MR reconstruction of the (110) surface is shown in Fig. 1. The closed-packed rows run along the $[\bar{1}10]$ direction. The missing-row reconstruction exposes atoms in the third layer of the crystal. The microfacets formed by the three different rows constitute part of a (111) plane.

We will first address the question of the basic model for the observed (1×3) reconstruction. The observed LEED pattern can be rationalized with models that range from lateral translations in the top layer of a bulk-terminated

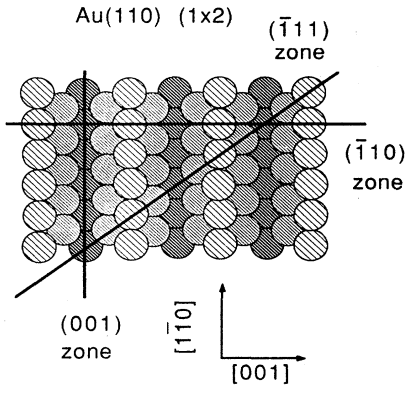

FIG. 1. Top view of the Au(110)-(1×2) surface (missing-row structure). The scattering planes used below are indicated.

structure to models with a different number of vacancies in the first few layers of the crystal. The different scattering geometries will provide information on the qualitative features of the structure that will help us to narrow down the set of possible models. Once the general geometrical model has been found, the next step is to determine the changes in the atomic positions away from their bulk values.

Different scattering geometries are sensitive to different structural parameters. Data were therefore collected in three different planes (Fig. 1), namely, the $(\bar{1}10)$, the $(\bar{1}11)$, and the (001) zones.

The data for the $(\bar{1}10)$ zone are shown in Fig. 2(a). The ion beam was incident along the $[\bar{1}\,\bar{1}\,2]$ direction. In this geometry, there are two nonequivalent scattering planes, one terminating in the top layer and another in the second layer [Fig. 2(b)]. For a static, bulk-terminated (1×1) surface, the yield will be 2 atoms/unit-cell at any scattering angle. Vibrations will, at room temperature, increase this limit to approximately 2.2 atoms/unit-cell in single alignment and distortions (displacements laterally or perpendicular to the surface) will further increase this number. The data in Fig. 2(a) show pronounced blocking dips close to the [114], [116], and [1 1 12] bulk crystallographic directions. The fact that the experimental yield [Fig. 2(a)] goes well below 2.2 atoms/unit-cell around these dips is a clear indication that there are vacancies in the top layer.[6] These vacancies allow the ions to penetrate into the crystal. The backscattered flux is then prevented from reaching the detector by blocking from the remaining surface atoms. By this argument we can discard all models based on a bulk-terminated structure (i.e., models with the same number of atoms in the top layer as in any bulk layer), with or without distortions. In Figs. 2(b)–2(e) we show instead several possible models with the correct characteristics.

The blocking dip observed in the [116] direction is a common feature to all of these models. It is due to ions scattered from atoms in the third and fourth layers, which are blocked by atoms in the first and second layers, as indicated in Figs. 2(b)–2(e). The (1×3) surface symmetry implies that a very similar argument also explains the blocking dip in the [1 1 12] direction.

We also observe a very pronounced [114] blocking dip. This is unexpected, since the incident ion beam cannot hit the specific atoms which will produce blocking along the [114] direction for any of the models shown above [Figs. 2(b)–2(e)] *if the atoms are located in bulklike positions.* This difficulty can be removed by invoking a large displacement perpendicular to the surface of the first layer, so that the third-layer atoms involved in the [114] blocking are effectively moved out of the shadow cone. The blocking dips in this zone are all shifted significantly towards smaller scattering angles. This behavior is very different from what has earlier been observed on Au(110) (Ref. 3) and Pt(110) (Ref. 6), where very small shifts were observed in this scattering geometry. The shifts are to smaller angles [Fig. 2(a)], which indicates that the displacement is a contraction. As the scattering in this zone is a measure of d_{13}, this indicates a significant difference between the (1×2) and the (1×3) surface: There has

been a quite significant change in this quantity between the two surfaces. The data below will give direct and independent evidence for this distortion.

For atoms in bulklike positions we also expect blocking dips along the [118] and the [1 1 10] directions, but these are not observed. The Monte Carlo simulations (see below) show that there is a large buckling of the third layer. Our simulations show that this smooths out the [118] blocking dip, leaving only a small step in the scattering yield around 44° [Fig. 2(a)]. The simulations also show that the distortions shift the [1 1 10] blocking dip to lower scattering angles so that it overlaps the [1 1 12] blocking dip, and contributes to the strong reduction of the yield around 41° in the data [Fig. 2(a)].

In order to select the correct model from the options presented above, it is necessary to examine other scattering zones. The normalized data from the $(\bar{1}11)$ scattering zone are shown in Fig. 3(a). The ion beam was incident along the $[0\bar{1}1]$ direction and detected near [101]. In this zone all atoms are included in one single scattering plane. The bulk blocking direction is at 60°, and a shift of the blocking dip towards smaller (larger) scattering angles is therefore indicative of a contraction (expansion) of the first interlayer distance. The data show a pronounced blocking dip at a scattering angle close to 56°. This is therefore direct evidence that the top layer is contracted towards the bulk.

The yield from the (1×3) surface in double alignment is very similar to that from the (1×2) surface [Fig. 3(a)], but the single alignment yield for the (1×3) surface is higher. This is indicative of a larger corrugation of the (1×3) surface. If the atoms were located in bulklike po-

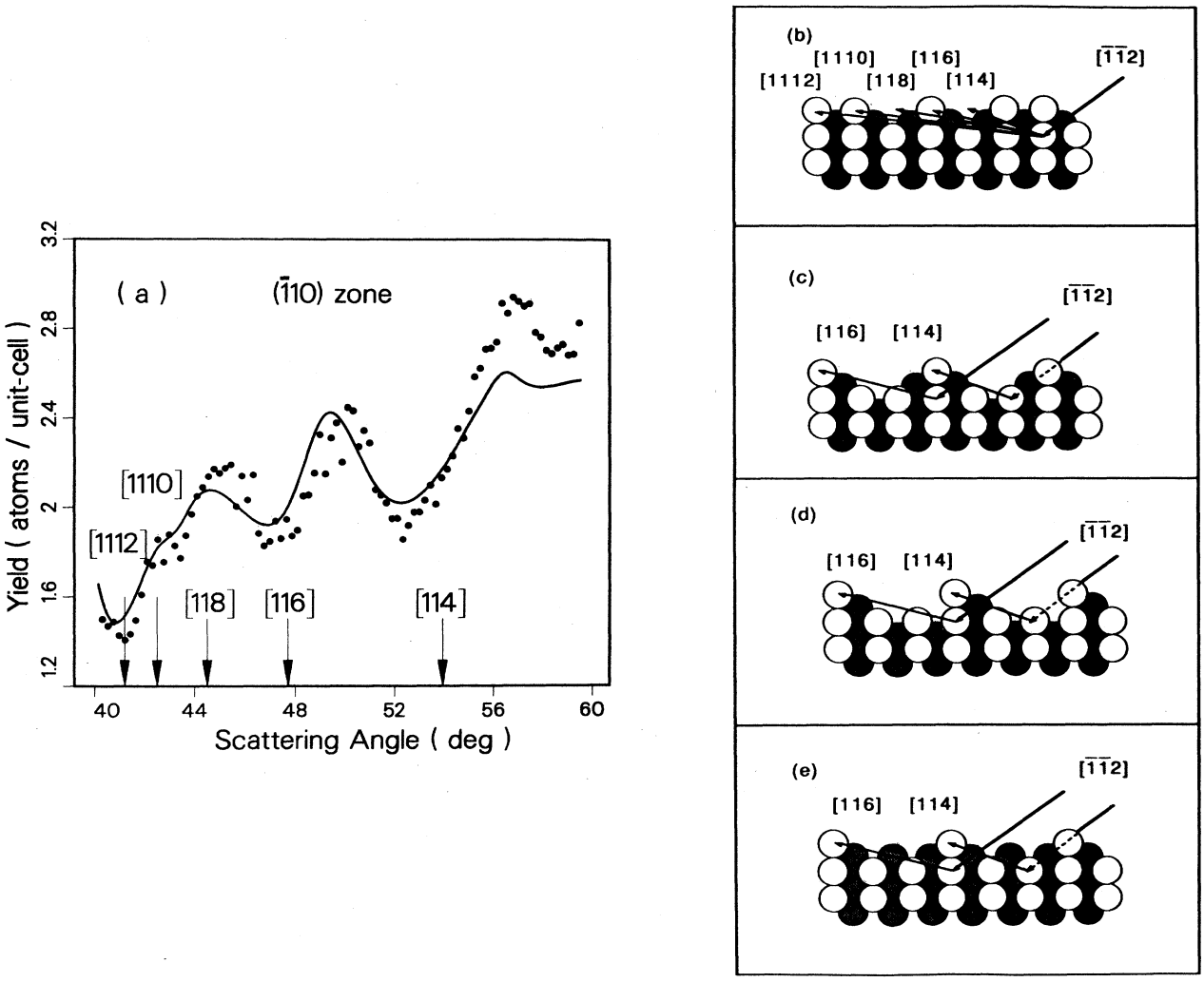

FIG. 2. (a) Channeling and blocking data, obtained in the $(\bar{1}10)$ scattering plane, for the Cs-induced (1×3)-reconstructed Au(110) surface. The proton energy was 65 keV and the ions were incident along the $[\bar{1}\,\bar{1}\,2]$ direction. The backscattered surface yield [in units of atoms per (1×1) unit cell] is plotted as a function of scattering angle. The bulk crystallographic directions are indicated with arrows. A simulation for the model determined below is shown as a solid line. (b)–(e) Side view of the $(1\bar{1}0)$ scattering plane for various models for the (1×3) reconstruction. Different shadings correspond to atoms located in different planes. The arrows indicate some of the possible blocking directions.

sitions, the single alignment yield would be the same for the two structures, but the blocking dip for the (1×3) surface would be deeper. We observe instead that the (1×3) single alignment yield is higher than the (1×2) yield. Therefore, the atoms in the (1×3) surface are further away from their bulklike positions than in the (1×2) surface. It is not difficult to see that this can be consistent with an unchanged double alignment yield.

One important feature of the data in the ($\bar{1}11$) zone is the depth of the blocking dip [Fig. 3(a)]. If the atoms were located in bulklike positions, the models in Figs. 3(b) and 3(e) would show a blocking dip shallower than the (1×2) MR structure [Fig. 3(f)] and should therefore be discarded. In the presence of the first-layer contraction, we should also consider this distortion in our qualitative analysis. The inspection of the models above show that also the model in Fig. 3(b) will exhibit a significant increase in the depth of the blocking dip due to this inwards displacement of the first layer. From this qualitative analysis we can conclude that only the model in Fig. 3(e) can be strictly eliminated, even in the presence of large surface distortions. The remaining models will be reexamined below in other scattering geometries.

The data presented so far show unambiguous evidence for vacancies in the top layer(s), and a large contraction of the first interlayer distance. Data obtained from the ($\bar{1}11$) zone but with the ion beam incident normal to the crystal [Fig. 4(a)] show the same qualitative features. The

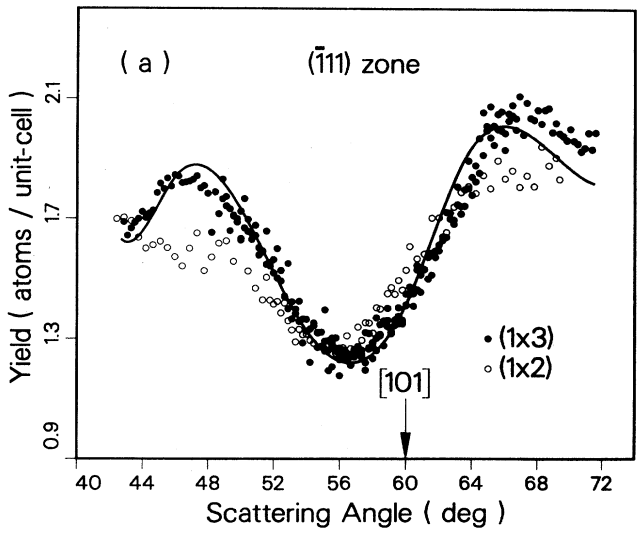

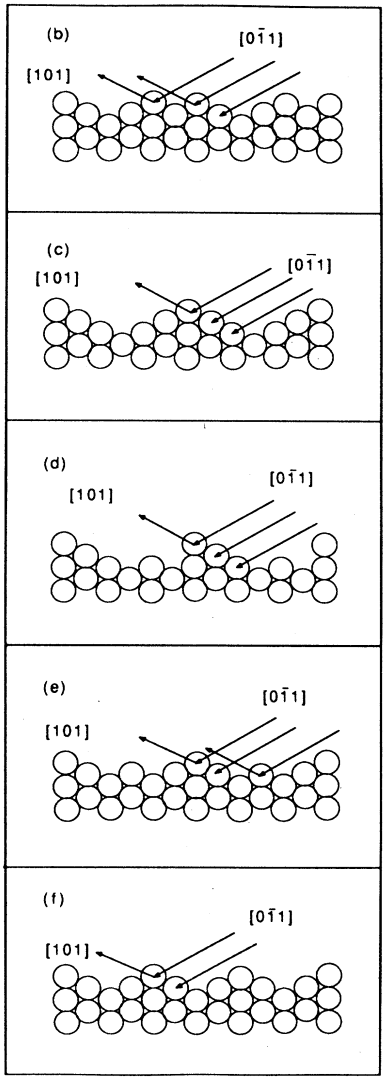

FIG. 3. (a) Experimental yield for 65-keV protons incident in the ($\bar{1}11$) zone along [$0\bar{1}1$] as a function of scattering angle. The data for the (1×3) surface are shown with solid circles, while the data for the (1×2) surface are given by open circles. Note that the blocking dip minimum is shifted with respect to the bulk [101] crystallographic direction. A simulation of our best structure (solid line) is also shown. (b)–(e) A side view of the ($\bar{1}11$) scattering plane in different models. The arrows indicate allowed ion propagation directions in double alignment. (f) A side view of the (1×2) surface in this zone.

ions were incident along the $[\bar{1}\,\bar{1}\,0]$ direction and detected near [101]. The bulk blocking direction is at 120° and the surface blocking dip is shifted to smaller scattering angles. This confirms the contraction of the top layer observed in Fig. 2(a) and again in Fig. 3(a). These data also show a deeper blocking dip than in the previous scattering geometry [Fig. 3(a)]. To understand why this is the case we will consider the models shown in Figs. 4(b)–4(d). The arrows in these figures picture the trajectories of the ions as they are backscattered from the surface along the [101] blocking direction. We see in Fig. 4(b) that three atoms for every three unit cells are being blocked, or the blocking dip for this geometry would be 1.0 atom/(1×1)-unit-cell deep, a value that compares very well with the size of the blocking dip displayed by the data in Fig. 4(a). The same is true for the model in Fig. 4(c). For the model in Fig. 4(d), instead, there is a larger number of atoms being blocked, making this model unsuitable to describe the data. In this way we have narrowed down the possible models to two [Figs. 4(b) and 4(c)]. Models with a larger number of vacancies than those shown in Fig. 4 can be discarded because they will imply an even deeper blocking dip in the scattering yield of this zone.

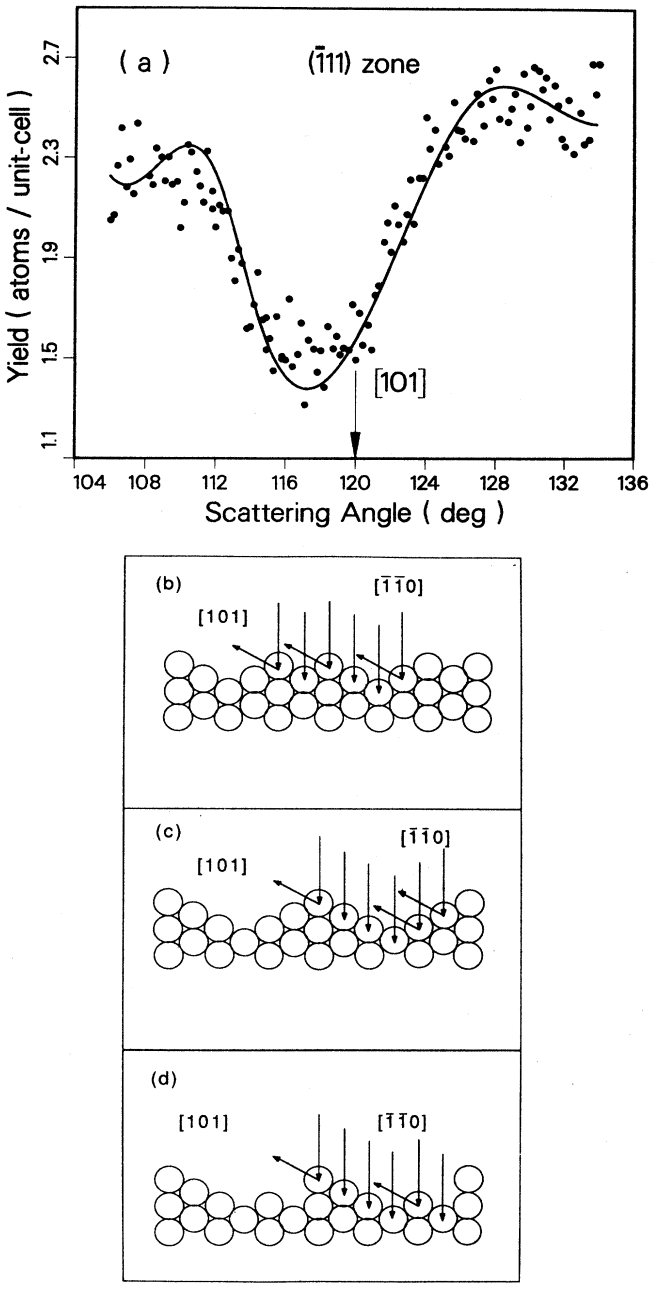

FIG. 4. (a) Experimental yield for 65-keV protons incident in the $(\bar{1}11)$ zone along the $[\bar{1}\,\bar{1}\,0]$ direction as a function of scattering angle. The bulk [101] blocking direction is indicated. The solid line is the simulation for the best structural model. (b)–(d) A side view of the $(\bar{1}11)$ plane in different models. The arrows indicate allowed ion propagation directions in double alignment.

Figure 5 shows data from the (001) zone with the ion beam incident along the $[0\bar{1}0]$ direction and the detector centered around the [100] direction. In this zone the scattering plane is parallel to the closed-packed rows. Since we do not expect vacancies within the rows, we have used higher-energy protons to probe the locations of the top-layer atoms relative to those further into the bulk. The two remaining models have, respectively, three and four nonequivalent scattering planes in this geometry, terminating in the first, second, etc., layers. The data show a blocking dip at a scattering angle close to the bulk value 90°. As we have already shown that some atoms are displaced large distances from their bulk positions, this observation indicates that there is averaging from the different sets of planes. The yield at the bottom of the blocking dip is 3.0 atoms/unit-cell. In the static bulk-terminated case, the scattering yield would be

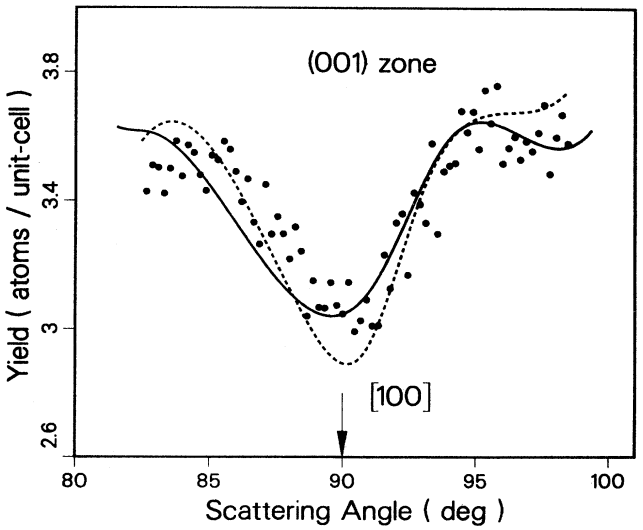

FIG. 5. Experimental yield for 180-keV protons incident along the $[0\bar{1}0]$ direction and detected around the bulk [100] direction in the (001) zone. The solid line is the simulation for the best structure. The two lines are simulations for two different models of the surface vibrations (see text).

2 atoms/unit-cell. As for the ($\bar{1}11$) zone [Fig. 4(a)], the data show a 50% increase with respect to this value.

One of the remaining models [Figs. 2(b), 3(b), and 4(b)] corresponds to a structure that joins together a (1×1) and a (1×2) unit cell to form the observed (1×3) LEED pattern. Monte Carlo simulations in the geometry of Fig. 3(a) yielded a set of surface distortions which gave reasonable agreement with the data. We then used variations around these parameters to simulate the scattering yield in the ($\bar{1}10$) zone. The results of these simulations were always inconsistent with the experimental data.

By this analysis we have covered a reasonable range of models and we consequently feel confident that there is strong evidence for the model with large corrugation formed by (111) microfacets. Top and side views of this model are shown in Figs. 6(a) and 6(b).

In order to quantify the distortions, extensive Monte Carlo simulations were performed. We allowed the first, second, and third interlayer spacings (d_{12}, d_{23}, and d_{34}, respectively) to vary, and kept the spacing between deeper layers fixed at the bulk value. As studies of the Au(110) (Refs. 2 and 3) and Pt(110) (Ref. 6) (1×2) surfaces have shown that a buckling of the third layer (B_3) may be important, we also allowed for such a distortion, as well as for lateral movements of the atoms (pairing, P_2) in the second layer.

As is usual in the analysis of MEIS data, we also allowed for an enhancement of the surface vibrational amplitudes. The description of the thermal vibrations is an important element in the Monte Carlo simulations.[1] The energies of the incident ions used in this experiment are such that the time of travel of each individual ion inside the crystal is at least three orders of magnitude shorter than the typical period of an atomic oscillation. This means that every scattered ion will "see" a different thermally distorted static lattice and the yield will be a strong function of the amplitude of the vibrations. The bulk one-dimensional vibrational amplitude of Au is, at 300 K, 0.087 Å. To take into account the correlation between the vibrational motion on adjacent atoms, we renormalize[20] this value by the known[21] bulk correlation coefficient, 0.3, which gives a renormalized vibrational amplitude of 0.072 Å.

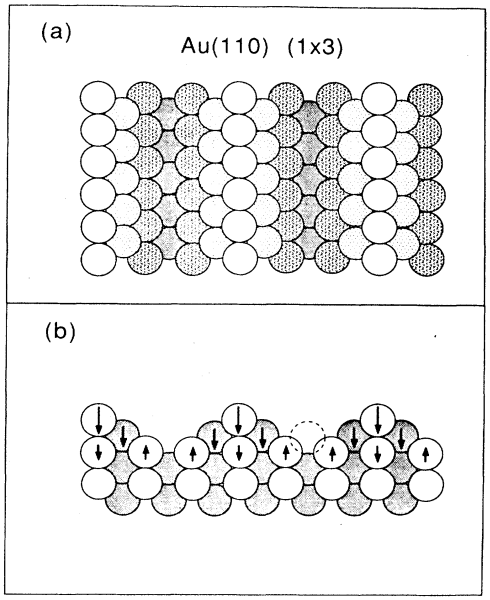

FIG. 6. Top (a) and side (b) view [in the ($\bar{1}10$) plane] of our model for the Au(110)-(1×3) surface. The arrows indicate the direction of movement of the atoms, relative to their bulklike positions.

Since the surface is drastically modified due to the reconstruction, it is not obvious how to model the surface vibrations. The unit cell considered in the calculations contains as many as 18 atoms. In principle, each one of these atoms should be assigned a different enhancement, so for isotropic vibrations this will mean including 18 different variational parameters in the simulations. The symmetry of the unit-cell reduces this number to 6. This is still too many, considering that we also have at least five structural parameters and that the computation time increases very rapidly with the total number of variational parameters. The only solution is to define a reasonable enhancement for each atom in the unit-cell. This definition was made through a function with one variational parameter. In this way we can generate different models to describe the surface vibrations by using different functions and only one adjustable parameter. We have described the vibrations in two different ways. In the first model, the enhancement of a particular atom was simply a function of the layer number [for the bulk terminated (1×1) surface], decaying exponentially towards the bulk with a decay constant of two layers. This kind of model has been used successfully for bulk-terminated surfaces[1] and for Au(110)-(1×2) and Pt(110)-(1×2).[3,6] Since the (1×3) model we consider is a wide open surface with long (111) facets instead of clearly defined layers of atoms, a second approach was also attempted. The enhancement was here taken to be a monotonically increasing function of the number of the neighboring vacancies. This enhances the vibrations of the atoms in the facets more than those not directly on the surface. In principle, this will make the surface stiffer than in the previous case, since fewer atoms will have their vibrations enhanced. Our structural results were not very sensitive to the exact description chosen. As an example we show in Fig. 5 the simulations for each vibrational model in the scattering zone most sensitive to the details of the vibrations; the (001) zone. The agreement between data and the calculated yield is similar for the two models, although the optimum numerical value for the enhancements of the vibrational amplitude were different.

Since the model under consideration has a very open surface it is reasonable to define the enhancement for the surface vibrations as the value obtained by averaging the atomic vibrational amplitudes over all the atoms in the (111) microfacets [i.e., all the atoms visible in Fig. 6(a)]. The surface vibrational amplitude obtained from the simulations is $\approx(0.130\pm0.028\pm0.022)$ Å. The first error

bar reflects the range of values for the enhancement, from the atom in the top layer to the fourth layer atom at the bottom of the trough. The second error bar is a reflection of the imperfections in the vibrational models and corresponds to the change in this average value obtained from the different scattering geometries.

As a result of the simulations we found a (very large) contraction of d_{12}, $\Delta d_{12} \approx (-22 \pm 4)\%$. The second interlayer distance d_{23} is also contracted: $\Delta d_{23} \approx (-9 \pm 3)\%$. Another major distortion is a buckling in the third layer; $B_3 \approx 0.14 \pm 0.04$ Å. The buckling is such that the atom immediately below the top row moves towards the bulk a distance of 0.07 Å from the relaxed third-layer position and the other two third-layer atoms in the unit cell move outwards by the same amount. We also found $P_2 \approx (-2 \pm 2)\%$, a result consistent with no pairing but with a very slight tendence to shorten the distance between the two atoms in the second layer located symmetrically below the top-layer atom. Another distortion of secondary importance is a contraction of the distance between the third and fourth atomic layers: $\Delta d_{34} = (-3 \pm 2)\%$. The net effect of all of these distortions is to produce a smoother surface than the undistorted (1×3) structure. The error bars quoted above reflect two factors: The differences between the optimal structural parameters in different zones and the range over which the parameters can be changed within a specific zone without causing a statistically significant change in the fit.

MEIS data for the Au(110)-(1×2) surface showed that $\Delta d_{12} = -18\%$.[3] While we find a larger value for the (1×3) surface (−22%), this difference is relatively minor. However, for the clean surface $\Delta d_{23} = +4\%$, as compared to −9% found above. This means that there is a very large change in d_{13}, which is needed to explain the strong [114] blocking dip in Fig. 2. Taking into account the effect of the change in d_{12}, as well as the effect of the buckling, this means that the nearest-neighbor bondlengths are contracted by 5 to 13 %. The magnitude of these distortions seems to imply an increase in the strength of the 5*d* bonding. Once the pressure of the *s-p* electrons has been relieved by the creation of the surface facets, the attractive *d* interaction induces important changes in the relaxations. A very similar result was recently obtained for the K-induced (1×2) reconstruction of Ag(110).[10] MEIS data for the clean Ag(110) surface have shown that $\Delta d_{12} = -9.5\%$, and $\Delta d_{23} = +6.0\%$,[22] in satisfying agreement with earlier high-energy ion scattering data.[23] Although d_{12} does not change much when the surface becomes reconstructed ($\Delta d_{12} = -9.0\%$), d_{23} does ($\Delta d_{23} = -1.0$).[10]

We have also investigated the effects of defects in the (1×3) model. The simplest modification to this model is to reinstate the row missing in the second layer. For simplicity, the atoms were assumed to be located in the relaxed position of the second-layer vacancy [Fig. 6(b)]. We allowed the percentage of the surface that displayed this feature to vary. At the same time we also varied the enhancement of the vibrational amplitudes (to compensate for changes in the yield that occur). From the data in the ($\bar{1}11$) zone (Fig. 3), we obtained the *R*-factor (reliability-factor) contour plot shown in Fig. 7. It has a flat minimum at a coverage of 3% of a monolayer of defects. In other zones, somewhat different values were obtained. For example, in the ($\bar{1}10$) zone [Fig. 2(a)] and in the (100) zone [Fig. 5(a)], a local minimum of the *R* factor was obtained for a coverage of 12%. Our conclusion based on this result is that there are noticeable imperfections on this surface, but since the effect of these defects in our calculations is small, we cannot determine their precise nature.

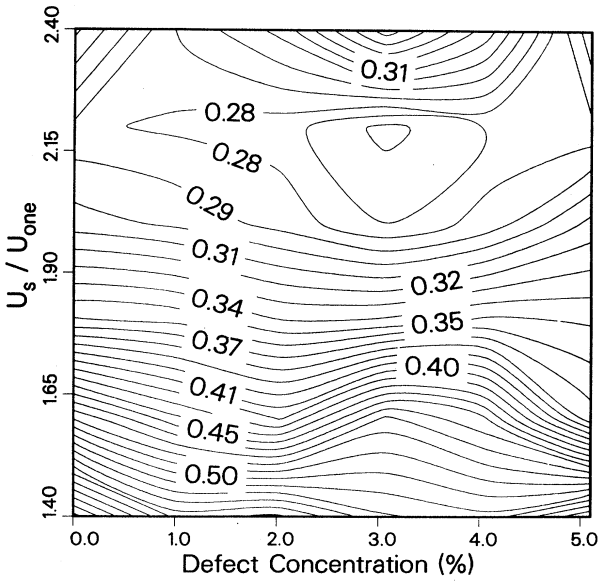

FIG. 7. *R*-factor plot for Monte Carlo simulations for the data in the ($\bar{1}11$) zone (Fig. 3). The horizontal axis is the concentration of defects located in the third layer [dotted circle in Fig. 6(b)], and the vertical axis is the ratio of the one-dimensional surface vibrational amplitude (u_s) to that of the bulk (u_{one}). The *R*-factor contours are in arbitrary units, and should not be compared to the *R* factors calculated in LEED.

The results from these simulations are shown by a solid line for each scattering geometry accompanying the experimental data [Figs. 2(a), 3(a), 4(a), and 5(a)]. The agreement is good in the ($\bar{1}11$) zones, both in normal [Fig. 4(a)] and [101] incidence [Fig. 3(a)]. For the (001) zone (Fig. 5) and the ($\bar{1}10$) zone [Fig. 2(a)] the simulations are not as close to the data, but considering the uncertainty of the models used to describe the surface vibrations we feel satisfied with the quality of the agreement obtained. It is always difficult to obtain good agreement in the ($\bar{1}10$) zone, as scattering in this geometry probes the structural coherence over large interatomic separations and is therefore very sensitive to defects.

IV. CONCLUSIONS

Inspection of MEIS data for the Cs-induced (1×3) reconstruction of Au(110) shows clear and direct evidence for a large number of vacancies, a substantial contraction of d_{12}, and a large change of d_{13} relative to the (1×2) surface. Monte Carlo simulations show that a generalized missing-row model with long (111) microfacets is the appropriate structure to describe this sur-

face.[15] The simulations further show a large contraction of the first interlayer distance, $\Delta d_{12} \approx (-22 \pm 4)\%$. The next most important distortion corresponds to a contraction of the second interlayer distance $\Delta d_{12} \approx (-9 \pm 3)\%$. This is an important change between the Cs-induced surface reconstruction and the clean surface,[2,3] where the same distance is expanded ($\Delta d_{23} \approx +4\%$). The (1×3) surface also has a significant buckling distortion of the third layer; $B_3 \approx 0.14 \pm 0.04$ Å. The relaxations are such that they make the surface smoother than the undistorted structure.

The proposed model for the (1×3) Cs-induced reconstruction belongs to a class of higher-order MR structures, which calculations have shown to have a very small difference in their total energy with respect to the "stable" (1×2) MR structure. We can understand this new reconstruction in terms of a change in the ground-state configuration induced by a charge transfer from Cs to the Au substrate. This study constitutes new experimental evidence supporting the hypothesis that these MR reconstructions are stabilized by the formation of long (111) microfacets.

ACKNOWLEDGMENTS

We would like to thank Dr. P. O. Nilsson for supplying the crystal used in this work. This research was supported by National Science Foundation (NSF) Grant No. DMR-87-03897. Use of the Central Facilities at the Laboratory for Research on the Structure of Matter at the University of Pennsylvania, under NSF Grant No. DMR-85-19059, is gratefully acknowledged.

[1]J. F. van der Veen, Surf. Sci. Rep. **5**, 199 (1985).
[2]W. Moritz and D. Wolf, Surf. Sci. **163**, L655 (1985).
[3]M. Copel and T. Gustafsson, Phys. Rev. Lett. **57**, 723 (1986).
[4]C.-M. Chan and M. A. Van Hove, Surf. Sci. **171**, 226 (1986).
[5]M. Copel, P. Fenter, and T. Gustafsson, J. Vac. Sci. Technol. A **5**, 742 (1987).
[6]P. Fenter and T. Gustafsson, Phys. Rev. B **38**, 10 197 (1988).
[7]B. E. Hayden, K. C. Prince, P. J. Davy, G. Paolucci, and A. M. Bradshaw, Solid State Commun. **48**, 325 (1983).
[8]M. Copel, W. R. Graham, T. Gustafsson, and S. Yalisove, Solid State Commun. **54**, 695 (1985).
[9]C. J. Barnes, M. Q. Ding, M. Lindroos, R. D. Diehl, and D. A. King, Surf. Sci. **162**, 59 (1985).
[10]J. W. M. Frenken, R. L. Krans, J. F. van der Veen, E. Holub-Krappe, and K. Horn, Phys. Rev. Lett. **59**, 2307 (1987).
[11]K.-M. Ho and K. P. Bohnen, Phys. Rev. Lett. **59**, 1833 (1987).
[12]S. M. Foiles, Surf. Sci. **191**, L779 (1987).
[13]J. W. Davenport and M. Weinert, Phys. Rev. Lett. **58**, 1382 (1987).
[14]Murray S. Daw, Surf. Sci. **166**, L161 (1986).
[15]M. Garofalo, E. Tosatti, and F. Ercolessi, Surf. Sci. **188**, 321 (1987); F. Ercolessi, A. Bartolini, M. Garofalo, M. Parrinello, and E. Tosatti, Surf. Sci. **189/190**, 636 (1987).
[16]W. Moritz and D. Wolf, Surf. Sci. **88**, L29 (1979).
[17]G. A. Held *et al.* (private communication).
[18]A. Morgante, K. C. Prince, G. Paolucci, and E. Tosatti, Surf. Sci. **189/190**, 620 (1987).
[19]W. R. Graham, S. M. Yalisove, E. D. Adams, T. Gustafsson, M. Copel, and E. Törnqvist, Nucl. Instrum. Methods B **16**, 383 (1986).
[20]D. P. Jackson, T. E. Jackman, J. A. Davies, W. A. Unertl, and P. D. Norton, Surf. Sci. **126**, 226 (1983).
[21]S. P. Withrow, J. H. Barrett, and R. J. Culbertson, Surf. Sci. **161**, 584 (1985).
[22]E. Holub-Krappe, K. Horn, J. W. M. Frenken, R. L. Krans, and J. F. van der Veen, Surf. Sci. **188**, 335 (1987).
[23]Y. Kuk and L. C. Feldman, Phys. Rev. B **30**, 5811 (1984).